Plasma Crystal Melting: A Nonequilibrium Phase Transition

V. A. Schweigert,[1] I. V. Schweigert,[2] A. Melzer,[3] A. Homann,[3] and A. Piel[3]
[1]*Institute of Theoretical and Applied Mechanics, Novosibirsk, Russia*
[2]*Institute of Semiconductor Physics, Novosibirsk, Russia*
[3]*Institut für Experimentelle und Angewandte Physik, Christian-Albrechts-Universität, 24098 Kiel, Germany*
(Received 18 November 1997)

The plasma crystal is shown to exhibit a nonequilibrium two-step phase transition due to particle heating by ion streaming motion in the sheath. In a nonlinear model, the energy increase due to an ion induced instability is found to be separated from the melting transition. The plasma crystal melts at a much higher particle energy than expected from classical models. This behavior is explained by preferred destabilization of short-wavelength modes in the plasma crystal. [S0031-9007(98)06350-9]

PACS numbers: 52.35.−g, 52.25.Vy, 64.60.−i

Plasma crystals represent a unique bridge connecting the fields of (nonideal) plasmas and condensed matter physics. Plasma crystals consist of micrometer sized particles trapped in the space charge sheath of magnetron or parallel plate rf discharges, where the particles form flat, nearly two-dimensional (2D) ordered structures [1–3]. The fast response and their easy observability allow one to study details of the phase transitions within actual time scale. Melting transitions of 2D systems have been studied theoretically under equilibrium conditions for the past two decades [4]. Nonequilibrium phase transitions have also been found experimentally and theoretically in colloidal suspensions, where ordering of the particles has been induced by shear flows, optical gradients, or electrophoresis [5], and they have been investigated in view of spatial and temporal pattern formation [6].

Plasma crystals having two or more layers undergo a phase transition from an ordered, vertically aligned, hexagonal structure via a liquid to an almost gaslike state when the gas density in the discharge is reduced [7,8]. In the space charge sheath the ions flow at supersonic speed from above through the plasma crystal forming regions of enhanced ion density (ion clouds) in the wake below the dust particles [9–13]. Experiments and linear analysis of this situation [9,10] show that the ion clouds provide an attractive force leading to the observed vertical alignment. The alignment becomes unstable below a certain threshold of the discharge gas density, where characteristic oscillations set in, which lead to the heating of the particles and which have been observed in the experiment. Because of the supersonic ion flow, the plasma crystal represents an *open* system, in which a nonequilibrium phase transition occurs. In colloidal suspensions ordering of the particles has been found under nonequilibrium conditions [5], whereas here, depending on the strength of nonequilibrium behavior, ordered and fluid structures exist.

Recently, Melandsø [13] has studied the relaxation of a perfect 3D infinite dust crystal in a quasineutral plasma with constant supersonic ion flow into a liquid state for two values of the neutral gas friction, where the ion instability saturates before and after melting of the crystal, respectively, indicating that melting occurs in a two-step process.

In this Letter, the melting transition of the plasma crystal is investigated in the space charge sheath with continuously reducing the gas density in a nonlinear model for the dust dynamics, thereby closely following the experimental procedure given in [7]. In contrast to the idealized 3D system in [13], here a bilayer crystal with hexagonal structure in the horizontal plane and vertically aligned particles is studied (see also Fig. 1) with an interparticle distance of $a = 450\ \mu$m, an interlayer distance of $d = 360\ \mu$m, a particle charge of $Z = 13\,000$ elementary charges, and a particle mass of $M = 6.73 \times 10^{-13}$ kg. The self-excited oscillations observed in the experiment have a frequency close to the dust plasma frequency $\omega_{\mathrm{pd}} = \sqrt{Z^2 e^2/\epsilon_0 M a^3}$ ($\omega_{\mathrm{pd}} = 90\ \mathrm{s}^{-1}$ for our conditions), and the motion is mostly in the horizontal direction. Hence, only particle motions in the horizontal plane $\vec{\rho}_{jk} = (x_{jk}, y_{jk})$ (at fixed vertical positions z_k) are considered in our model. The index j labels the particles in each plane and k corresponds to the upper ($k = 1$) and lower ($k = 2$) layer.

Forces on the dust particles are due to collisions with the neutral gas atoms, electrostatic interaction with the other particles, and the ion density distribution in the sheath. The actual density distribution of the streaming ions can

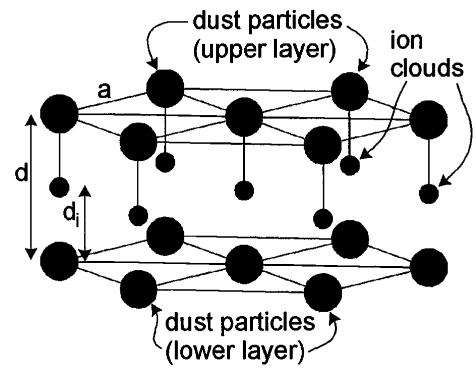

FIG. 1. A single cell of the simulated system.

be replaced by a positive point charge Z_i which is rigidly connected to each particle at a distance of $d - d_i$ below each particle [10]. The neutral gas exerts a friction force on the particles with friction constant ν. A Langevin force $\vec{F}_{\mathrm{L}}$ takes into account individual collisions of the neutral gas atoms with the dust particles. The Langevin force here corresponds to a gas temperature of 300 K. The equation of motion for the particles can then be written as

$$\frac{d_{jk}^2 \vec{\rho}}{dt^2} = \frac{1}{M} \vec{F}_{jk} - \nu \frac{d\vec{\rho}_{jk}}{dt} + \frac{1}{M} \vec{F}_{\mathrm{L}} . \qquad (1)$$

The force $\vec{F}_{jk} = \vec{F}_{jk,\mathrm{pp}} + \vec{F}_{jk,\mathrm{pi}}$ consists of two parts. The first describes the repulsion due to the neighboring particles $\vec{F}_{jk,\mathrm{pp}} = -\partial U_{\mathrm{pp}} / \partial \vec{\rho}_{jk}$ with

$$U_{\mathrm{pp}} = \sum_{i>j} \sum_{k=1}^{2} U(\vec{\rho}_{ik} - \vec{\rho}_{jk}) + \sum_{ij} U(|\vec{\rho}_{i1} - \vec{\rho}_{j2} + \vec{e}_z d|) ,$$

where the first term on the right-hand side is the electrostatic interaction of particles in the same layer and the second is the repulsion of particles in different layers. $\vec{e}_z$ is the unit vector in the vertical direction. The second part, $\vec{F}_{jk,\mathrm{pi}} = -\delta_{k2} \partial U_{\mathrm{pi}} / \partial \vec{\rho}_{jk}$, describes the attractive force on the lower particles due to the ion distribution (replaced by a single point charge) which can be written as

$$U_{\mathrm{pi}} = -\epsilon \sum_{ij} U(\vec{\rho}_{i1} - \vec{\rho}_{j2} + \vec{e}_z d_i), \qquad \epsilon = Z_i / Z .$$

Here, $\epsilon = 0.5$ and $d_i = 0.4a$ will be used [10]. The Kronecker symbol δ_{k2} ensures that the attraction is only on the particles of the lower layer. A similar force does not exist for the upper layer because, in the supersonic ion flow, an attractive force by polarization of the ion flow can only be communicated in the flow direction. This asymmetry is the reason for the instability and the nonequilibrium behavior of the system [9]. This situation can also be viewed as a classical analogon to Cooper pairing [11].

The particle interaction potential U is assumed to be of a Debye-Hückel-type,

$$U(\vec{\rho}_i - \vec{\rho}_j) = \frac{e^2 Z^2}{4\pi\epsilon_0 |\vec{\rho}_i - \vec{\rho}_j|} \exp(-\lambda |\vec{\rho}_i - \vec{\rho}_j| / a) ,$$

where λ is the effective screening strength. $\lambda = 0$ describes the pure Coulomb potential. In this Letter we mainly present results for $\lambda = 2$, which is close to experimental findings [14].

From the linear analysis [10] it is known that, due to the ion flow through the dust crystal, energy is drained from the flow and transferred to the dust particles. This can happen because of the (nonreciprocal) Coulomb interaction between the dust particles and the polarized ion flow. If the neutral gas density is high enough, the energy transferred to the particles is dissipated by friction with the neutral gas. When the friction constant drops below a critical value ($\nu_{\mathrm{in}} = 0.1635\omega_{\mathrm{pd}}$ for the conditions here) the energy of the dust particles cannot be dissipated totally, and the vertically aligned particle arrangement becomes unstable leading to horizontal oscillations of the particles at a frequency of $\omega_{\mathrm{in}} = 0.88\omega_{\mathrm{pd}}$ and a wave vector of $\vec{q}_{\mathrm{in}} a = \frac{1}{2} q_{\mathrm{in}} a(\sqrt{3}, 1)$, $q_{\mathrm{in}} a = 2\pi/\sqrt{3}$ for the Debye-Hückel case.

In the nonlinear model a set of 448 particles (224 particles in each plane) with periodic boundary conditions is studied to analyze the phase transition. The Langevin equation was solved using a standard approach [15]. Starting with a hexagonal vertically aligned structure the phase transition was studied by reducing the friction constant ν in the range between $0.5\omega_{\mathrm{pd}}$ and $0.1\omega_{\mathrm{pd}}$. This corresponds to the range of pressures between 140 and 30 Pa in helium, where the experiments [7] were performed.

The particle trajectories, calculated from the model, are shown in Fig. 2 for different values of the friction constant. The corresponding energy E and Coulomb coupling parameter $\Gamma = Z^2 e^2 / 4\pi\epsilon_0 a E$ of the dust particles can be seen in Fig. 3. For high friction the particles move only slightly about their equilibrium positions exhibiting some irregular motion [Fig. 2(a)]. With reduced friction the particle trajectories become more and more irregular, but still form an ordered structure [Figs. 2(b) and 2(c)]. For the lowest value of ν this structure is destroyed and a fluid phase can be seen in Fig. 2(d). The particle energy increases dramatically from nearly room temperature to about 10 eV for the upper layer and 30 eV for the lower layer near $\nu_{\mathrm{in}} / \omega_{\mathrm{pd}} = 0.1635$ which is the onset of the instability in the linear model. In a narrow regime just below ν_{in} a very interesting feature of particle motion can be seen in Fig. 2(b), where a coherent motion of all particles is found, i.e., all particles have the same oscillation amplitude, phase, and frequency. However, as will be

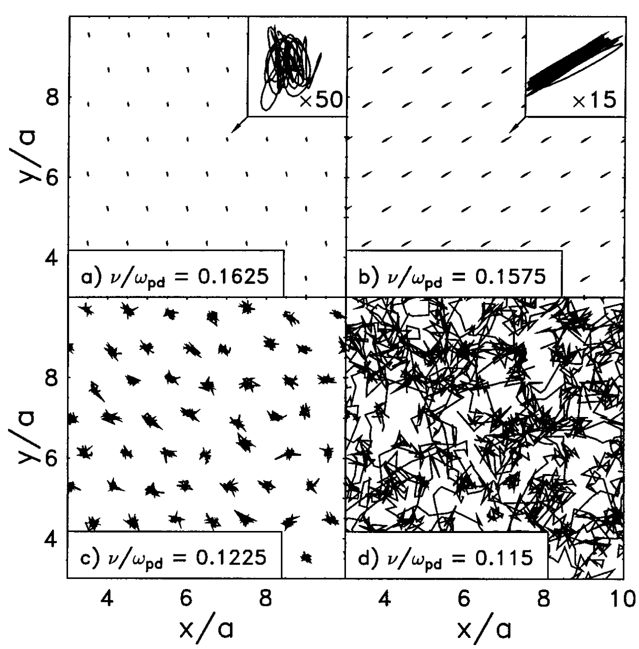

FIG. 2. The trajectories of the particles of the upper layer for $\lambda = 2$ and different friction constants. Note that the melting occurs between $\nu/\omega_{\mathrm{pd}} = 0.1225$ and $\nu/\omega_{\mathrm{pd}} = 0.115$.

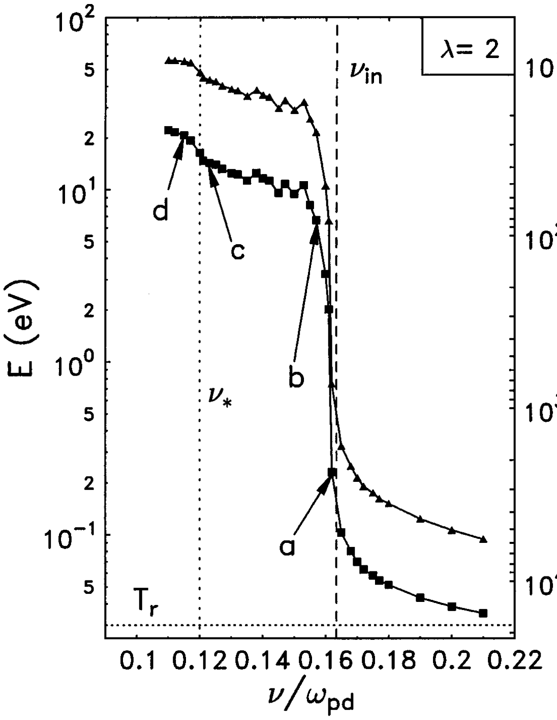

FIG. 3. The mean kinetic energy of the particles of the upper layer (squares) and the lower layer (triangles) for the Debye-Hückel interaction with $\lambda = 2$. The vertical dashed and dotted lines show the critical frictions corresponding to crystal instability ν_{in} and melting ν_*, respectively. The labels (a) to (d) refer to the trajectories in Fig. 2.

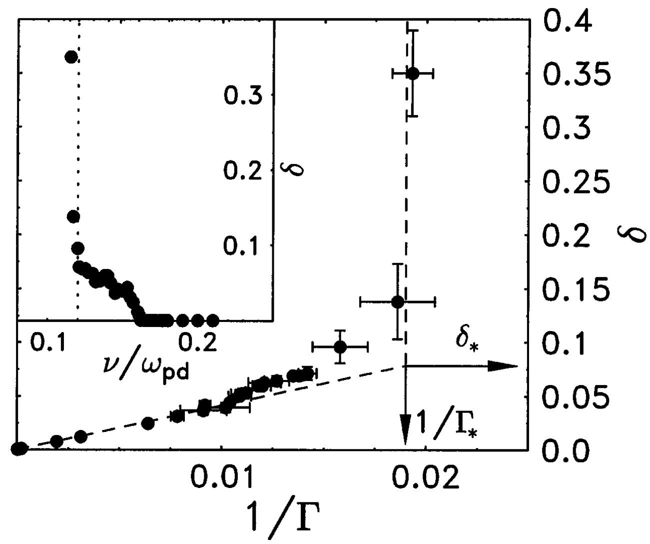

FIG. 4. The Lindemann parameter for particles of the upper layer for $\lambda = 2$ as a function of $1/\Gamma$. The inset shows the Lindemann parameter as a function of the friction constant. The vertical lines indicate the melting transition.

shown in more detail, the strong increase in the particles' energy near ν_{in} does not lead to the melting of the crystal. The melting occurs at an even further reduced friction of $\nu_* = 0.12\omega_{pd}$, where a second jump in temperature is found, leading to the fluid phase in Fig. 2(d). The corresponding particle energy and the friction constant for instability are close to that observed in experiments ($\nu_{in}/\omega_{pd} = 0.2$) [7]. Note also that, for $\nu > \nu_{in}$, the dust particles are already slightly heated above room temperature due to the ion flow.

The critical value of friction for the melting ν_* is determined from the modified Lindemann parameter [16]

$$\delta_k = \frac{2\pi}{\sqrt{3}} \frac{2}{Na^2} \left\langle \sum_{i=1}^{N/2} \frac{1}{N_b} \sum_{j=1}^{N_b} |\vec{u}_{ik} - \vec{u}_{jk}|^2 \right\rangle, \qquad (2)$$

where the second sum extends over N_b next neighbors. $\vec{u}_{jk}$ denotes the relative displacements of the particles from their equilibrium positions and $\langle\cdot\rangle$ is the average over time. The Lindemann parameter shows a sudden jump at $\nu_* = 0.12$ (see Fig. 4), indicating that the phase transition takes place only here. The critical Lindemann parameter for the transition is found to be $\delta_* = 0.08$ and the corresponding critical value of Γ is found to be $\Gamma_* = 52$ for the Debye-Hückel case $\lambda = 2$ ($\delta_* = 0.06$ and $\Gamma_* = 23$ for the Coulomb case $\lambda = 0$), which is much less than that expected for these systems [4].

The mode spectra Z_ω describing the phonon energy distribution during the transition, were calculated from the velocity autocorrelation functions

$$Z_{\omega,k}(\omega) = 2\int_0^\infty e^{i\omega\tau} Z_{v,k}(\tau)d\tau\,,$$

with $Z_{v,k}(\tau) = \sum_j \langle \vec{v}_{jk}(t)\vec{v}_{jk}(t-\tau)\rangle / \sum_j \langle \vec{v}_{jk}(t)\vec{v}_{jk}(t)\rangle$, where $\vec{v}_{jk}$ is the velocity of particle jk. The results are shown in Fig. 5. For the coherent regime at $\nu/\omega_{pd} = 0.1575$ just below the onset of instability at ν_{in}, the expected single-frequency spectrum is found [see Fig. 5(b)]. The excited mode has a frequency of $0.881\omega_{pd}$ which is very close to the most unstable mode found from the linear analysis. The linear analysis, however, shows that for the conditions here a large number of unstable modes in the frequency range between $0.847\omega_{pd}$ and $0.882\omega_{pd}$ should exist, but only a single narrow peak is seen in the spectrum. This type of nonlinear wave coupling is well known from many systems [6].

Figure 5(a) shows the spectra just above and just below the critical value for melting $\nu_* = 0.12$. The spectrum is broader than for the coherent regime, but the main contributions are still near $0.8\omega_{pd}$.

To check the reliability of our results we have also performed simulations on the phase transition of a single-layer crystal, which can be described by a Hamiltonian with the total energy $U_p = \sum_{ij} U(\vec{\rho}_i - \vec{\rho}_j)$. The critical value for the Coulomb coupling parameter was found to be $\Gamma_* = 189$ for $\lambda = 2$ ($\Gamma_* = 135$ for $\lambda = 0$) which is in agreement with the results of other simulations [4]. For the bilayer plasma crystal, however, $\Gamma_* = 52$ ($\Gamma_* = 23$) is found (see Fig. 4).

This large difference in the values of the critical coupling parameter can be explained by analyzing the autocorrelation spectra for a single-layer and a two-layer crystal.

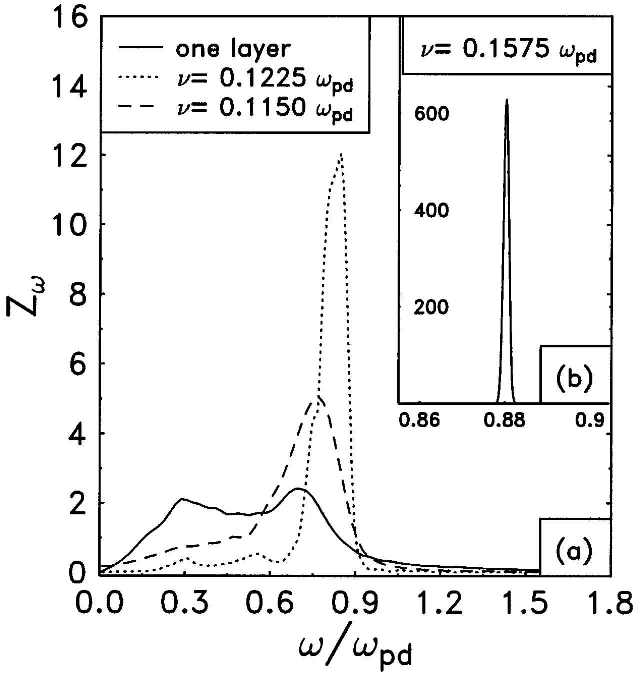

FIG. 5. The spectra of the velocity autocorrelation function for the Debye-Hückel potential for different friction constants. The solid curve corresponds to the spectrum of a single-layer crystal before melting ($\Gamma = 400$).

It is well known that long-wavelength (low-frequency) fluctuations play the key role for defect-mediated phase transition in 2D systems [4]. In Hamiltonian systems the phonon energy is uniformly distributed over the vibrational modes, which can also be seen in Fig. 5 for the single-layer crystal. In the plasma crystal, however, only modes close to the most unstable near $\omega = 0.8\omega_{\mathrm{pd}}$ are excited, and low-frequency modes are almost absent up to melting.

Using a harmonic approach, the critical Γ_* for the melting transition can be estimated from the spectra. There the frequencies and wave vectors of the modes in the autocorrelation spectra are assumed to be approximated by that of the most unstable mode at ω_{in} with wave vector $\vec{q}_{\mathrm{in}}$. The oscillation amplitudes A are related to the thermal energy of the particles via $MA^2\omega_{\mathrm{in}}^2/4 = E$. The displacements of the particles can then be written as $u_{jk} = A\cos(\vec{q}_{\mathrm{in}} \cdot \vec{\rho}_{jk} - \omega_{\mathrm{in}} t)$. Inserting this into Eq. (2) leads to

$$\Gamma_h = \frac{4\sqrt{\pi}}{3\delta_*}\left(\frac{2}{\sqrt{3}}\right)^{3/2}\left(\frac{\omega_{\mathrm{pd}}\sin(\sqrt{3}\,q_{\mathrm{in}}a/4)}{\omega_{\mathrm{in}}}\right)^2, \quad (3)$$

with the Lindemann parameters $\delta_* = 0.08$ ($\delta_* = 0.06$). This results in a critical value of $\Gamma_h = 49$ ($\Gamma_h = 19$), which is very close to $\Gamma_* = 52$ ($\Gamma_* = 23$) in Fig. 4. The harmonic approach for a single-layer crystal gives $\Gamma_h = 108$ for the Coulomb case [17]. Thus, the high-frequency components are responsible for the low value of Γ_* of the plasma crystal.

Similar low values of the critical coupling parameter ($10 < \Gamma_* < 60$) were reported in [13]. However, the strong spatial inhomogeneity of particle motion observed in [13] was neither seen in our experiments nor seen in the present simulations. The differences may be attributed to the assumption of an idealized quasineutral 3D crystal in [13] and of a flat 2D system embedded in a space charge sheath considered here.

In conclusion, we have presented a realistic nonlinear model of the nonequilibrium melting transition of the plasma crystal. The results may also be applicable to colloidal systems, where nonequilibrium situations due to shear flows, optical gradients, or electrophoretic forces lead to stringlike ordering effects [5], similar to the vertical alignment in plasma crystals due to the ion flow. It may be assumed that strong shear flows in colloidal systems result in similar phase transitions.

This work is partly supported by the Russian Foundation for Basic Research (96-02-19134-A), RFBR-DFG (96-02-00241-G/436 RUS 113/183/2), INTAS (94-740), and DFG (Pi185/8-2).

[1] J. H. Chu and I. Lin, Phys. Rev. Lett. **72**, 4009 (1994).
[2] H. Thomas *et al.*, Phys. Rev. Lett. **73**, 652 (1994).
[3] A. Melzer, T. Trottenberg, and A. Piel, Phys. Lett. A **191**, 301 (1994).
[4] K. Strandburg, Rev. Mod. Phys. **60**, 161 (1988).
[5] See, for example, W. Xue and G. S. Grest, Phys. Rev. Lett. **64**, 419 (1990); A. Larsen and D. G. Grier, Phys. Rev. Lett. **76**, 3862 (1996).
[6] H. Haken, *Synergetics* (Springer-Verlag, Berlin, 1978).
[7] A. Melzer, A. Homann, and A. Piel, Phys. Rev. E **53**, 2757 (1996).
[8] H. Thomas and G. E. Morfill, Nature (London) **379**, 806 (1996).
[9] A. Melzer *et al.*, Phys. Rev. E **54**, 46 (1996).
[10] V. A. Schweigert *et al.*, Phys. Rev. E **54**, 4155 (1996).
[11] S. V. Vladimirov and M. Nambu, Phys. Rev. E **52**, 2172 (1995); O. Ishihara and S. V. Vladimirov, Phys. Plasmas **4**, 69 (1997).
[12] F. Melandsø and J. Goree, Phys. Rev. E **52**, 5312 (1995).
[13] F. Melandsø, Phys. Rev. E **55**, 7495 (1997).
[14] S. Peters, A. Homann, A. Melzer, and A. Piel, Phys. Lett. A **223**, 389 (1996); A. Homann, A. Melzer, S. Peters, and A. Piel, Phys. Rev. E **56**, 7138 (1997).
[15] H. Gould and J. Tobochnik, *Computer Simulation Methods, Part 2* (Addison-Wesley, Reading, MA, 1987).
[16] V. M. Bedanov, G. V. Gadiyak, and Y. E. Lozovik, Phys. Lett. **109A**, 289 (1985).
[17] G. Goldoni and F. M. Peeters, Phys. Rev. B **53**, 4591 (1996).